doi:10.1093/brain/awx132 BRAIN 2017: 140; 2012–2027 | 2012

BRAIN
A JOURNAL OF NEUROLOGY

The Alzheimer's disease transcriptome mimics the neuroprotective signature of IGF-1 receptor-deficient neurons

Caroline George,[1,2] Géraldine Gontier,[1,2] Philippe Lacube,[1,2] Jean-Christophe François,[1,2] Martin Holzenberger[1,2] and Saba Aïd[1,2]

Seminal studies using post-mortem brains of patients with Alzheimer's disease evidenced aberrant insulin-like growth factor 1 receptor (IGF1R) signalling. Addressing causality, work in animal models recently demonstrated that long-term suppression of IGF1R signalling alleviates Alzheimer's disease progression and promotes neuroprotection. However, the underlying mechanisms remain largely elusive. Here, we showed that genetically ablating IGF1R in neurons of the ageing brain efficiently protects from neuroinflammation, anxiety and memory impairments induced by intracerebroventricular injection of amyloid-β oligomers. In our mutant mice, the suppression of IGF1R signalling also invariably led to small neuronal soma size, indicative of profound changes in cellular homeodynamics. To gain insight into transcriptional signatures leading to Alzheimer's disease-relevant neuronal defence, we performed genome-wide microarray analysis on laser-dissected hippocampal CA1 after neuronal IGF1R knockout, in the presence or absence of APP/PS1 transgenes. Functional analysis comparing neurons in early-stage Alzheimer's disease with IGF1R knockout neurons revealed strongly convergent transcriptomic signatures, notably involving neurite growth, cytoskeleton organization, cellular stress response and neurotransmission. Moreover, in Alzheimer's disease neurons, a high proportion of genes responding to Alzheimer's disease showed a reversed differential expression when IGF1R was deleted. One of the genes consistently highlighted in genome-wide comparison was the neurofilament medium polypeptide *Nefm*. We found that NEFM accumulated in hippocampus in the presence of amyloid pathology, and decreased to control levels under IGF1R deletion, suggesting that reorganized cytoskeleton likely plays a role in neuroprotection. These findings demonstrated that significant resistance of the brain to amyloid-β can be achieved lifelong by suppressing neuronal IGF1R and identified IGF-dependent molecular pathways that coordinate an intrinsic program for neuroprotection against proteotoxicity. Our data also indicate that neuronal defences against Alzheimer's disease rely on an endogenous gene expression profile similar to the neuroprotective response activated by genetic disruption of IGF1R signalling. This study highlights neuronal IGF1R signalling as a relevant target for developing Alzheimer's disease prevention strategies.

1 INSERM, Centre de Recherche Saint-Antoine, 75012 Paris, France
2 Sorbonne Universités, UPMC – Université Pierre et Marie Curie, 75012 Paris, France

Correspondence to: Martin Holzenberger,
Inserm UMR938, Faculté de Médecine, 27 rue Chaligny, F-75012 Paris, France
E-mail: martin.holzenberger@inserm.fr

Keywords: Alzheimer's disease; amyloid-β oligomers; hippocampus CA1; insulin-like growth factor receptor; transcriptome

Abbreviations: AβO = amyloid-β oligomer; KO = knockout

Received November 11, 2016. Revised March 31, 2017. Accepted April 12, 2017. Advance Access publication June 8, 2017

Introduction

Increased life expectancy in the modern world exposes more and more humans to age-related diseases. Investigating the complex mechanisms of ageing provided strong evidence that blocking insulin-like growth factor (IGF) pathways prolongs lifespan in various species, including mammals (Holzenberger *et al.*, 2003; Kappeler *et al.*, 2008; Kenyon, 2010; Xu *et al.*, 2014; Milman *et al.*, 2016). Recently, inhibition of IGF1 and its principal regulator growth hormone has been proposed as a promising strategy to retard human ageing and extend healthy lifespan (Longo *et al.*, 2015). Importantly, interventions slowing down ageing also postpone age-related pathologies, including Alzheimer's disease (Cohen *et al.*, 2006; Florez-McClure *et al.*, 2007), the most common neurodegenerative pathology. Alzheimer's disease is characterized by extracellular amyloid-β deposits and intracellular inclusions of tau aggregates that ultimately cause progressive, and so far irremediable decline of cognitive functions. Cohen *et al.* (2009) showed that lifespan-extending heterozygous IGF1R knockout (KO) confers neuroprotection and improves behaviour in Alzheimer's disease mice (Cohen *et al.*, 2009). In the brains of Alzheimer's disease patients, abnormalities in insulin like growth factor 1 receptor (IGF1R) expression and downstream signalling molecules, coupled with insulin and IGF1 resistance have also been demonstrated, although causality remains unclear (Steen *et al.*, 2005; Moloney *et al.*, 2010; Bomfim *et al.*, 2012; Talbot *et al.*, 2012). Indeed, evidence is accumulating that long-term blockade rather than enhancement of IGF signalling supports neuronal function and neuroprotection (Freude *et al.*, 2009; Gontier *et al.*, 2015; Gazit *et al.*, 2016; De Magalhaes Filho *et al.*, 2017). We found recently that deleting IGF1R from adult neurons of young APP/PS1 mice protected them lifelong from Alzheimer's pathology by clearing toxic amyloid-β via preserved autophagic compartment and enhanced systemic elimination (Gontier *et al.*, 2015). Together, these findings suggested strong mechanistic involvement of neuronal IGF signalling in Alzheimer's disease progression. However, interventional and systematic approaches to a better understanding of the interaction between Alzheimer's disease progression and IGF signalling in neurons are missing. Here, we report that neuron-specific deletion of IGF1R, even when performed in old mice, still protected against amyloid-β oligomer (AβO)-induced memory impairment and neuroinflammation. Using microarray analysis we compared transcriptional responses of hippocampal neurons in the early stages of Alzheimer's disease with neurons deprived of IGF signalling *in vivo*. This showed that highly overlapping molecular pathways were affected in the same direction in both conditions, especially those involved in neurotransmission, cellular stress response and cell growth. We also identified a set of IGF-dependent pathways that orchestrate neuroprotective mechanisms against amyloid-β proteotoxicity in adult Alzheimer's disease neurons.

Materials and methods

Animal models

CaMKIIα-CreER$^{T2+/0}$;IGF1R$^{flox/flox}$ and APPswe/PS1dE9$^{+/0}$; CaMKIIα-CreER$^{T2+/0}$;IGF1R$^{flox/flox}$ transgenic mice were generated as described (Gontier *et al.*, 2015). Briefly, APPswe/PS1dE9 and CaMKIIα-CreER^{T2} transgenes were backcrossed to IGF1R$^{flox/flox}$ knock-in mice to obtain APPswe/PS1dE9$^{+/0}$; IGF1R$^{flox/flox}$ and CaMKIIα-CreER$^{T2+/0}$;IGF1R$^{flox/flox}$ breeders. These two mutant genotypes were crossed to generate CaMKIIα-CreER$^{T2+/0}$;IGF1R$^{flox/flox}$ and APPswe/PS1dE9$^{+/0}$; CaMKIIα-CreER$^{T2+/0}$;IGF1R$^{flox/flox}$ mice. Male and female mice were used. As no major differences prevailed between sexes, results are displayed together, except for amyloid-β enzyme-linked immunosorbent assay (ELISA; see below). Mice were housed in individually ventilated cages, enriched with a red polycarbonate shelter (Tecniplast) and a cotton pad. The maximum number of mice per cage was five males or six females. Mice were kept on a 12/12 h light/dark cycle at 22°C room temperature, and free access to water and standard mouse chow (LASQCdiet Rod16, Genobios). To induce neuron-specific IGF1R knockout, CaMKIIα-CreER$^{T2+/0}$; IGF1R$^{flox/flox}$ and APPswe/PS1dE9$^{+/0}$;CaMKIIα-CreER$^{T2+/0}$; IGF1R$^{flox/flox}$ mice were injected intraperitoneally with tamoxifen twice per day for 5 consecutive days (42 mg/kg body weight per injection), resulting in inIGF1RKO and ADINKO conditional mutant mice, respectively. Tamoxifen (T5648, Sigma-Aldrich) was dissolved in sunflower seed oil/ethanol (10:1) at 10 mg/ml. Littermate control mice of the same genotypes were injected with vehicle alone. Efficiency of Cre-loxP recombination was systematically checked post-mortem in brain biopsies by PCR. This study was conducted in accordance with the guidelines for care and use of laboratory animals and European Community rules (86/609/EEC). All experiments were performed with the approval of *Comité d'Éthique pour l'Expérimentation Animale* "Charles Darwin" (specific approval Ce5/2012/043 and 01166.02).

Genotyping

DNA was isolated from tissue biopsies and subjected to multiplex PCR as described (Gontier *et al.*, 2015).

Amyloid-β oligomers

AβOs were prepared from synthetic peptide amyloid-β42 (Tocris Bioscience); phosphate-buffered saline (PBS) or reverse peptide amyloid-β42-1 were used as controls as described (Choi and Bosetti, 2009; Santos *et al.*, 2012). Briefly, peptides were dissolved at 0.1 mg/ml in 99% hexafluoroisopropanol (HFIP) (105228, Sigma-Aldrich). HFIP was evaporated to obtain dry films that were resuspended in PBS at 1 μg/μl and incubated at 37°C for 48 h. AβOs were used within 12 h of preparation. AβOs were characterized by western blot using anti-amyloid-β 6E10 antibody (not shown) and by transmission electron microscopy.

Intracerebroventricular injections

Twenty-five-month-old inIGF1RKO and control mice were anesthetized by intraperitoneal injection of 100 mg ketamine and 10 mg xylazine per kg body weight. We administered 400 pmol of AβOs (aggregated from amyloid-β42) or vehicle (PBS) into the lateral ventricle (Aid *et al.*, 2008). Stereotaxic coordinates were −0.5 mm antero-posterior, −1.0 mm medio-lateral, −2.3 mm dorso-ventral from bregma (Paxinos and Franklin, 2013). AβOs were injected with a 10 µl microsyringe fitted with 33-gauge needle and automated syringe pump (Stoelting) at 0.5 µl/min, in a final volume of 4 µl. After delivery, the needle was kept in place for 5 min to prevent backflow.

Barnes maze test

All behavioural experiments were performed in a dedicated room between 9 am and 6 pm, alternating experimental groups throughout this interval. The Barnes maze was used to assess spatial learning and memory as described (Gontier *et al.*, 2015). Mice were trained four times per day for four consecutive days to escape from a brightly lit circular platform into a refuge box hidden beneath the target hole (one of the 20 holes positioned along the perimeter). Each trial lasted up to 5 min with an intertrial interval of at least 15 min. The maze was cleaned with 70% ethanol after each trial. On Day 5, long-term memory retention was evaluated during a 3-min session. Latency, errors (wrong hole) and distance travelled were recorded by automated video tracking (Viewer^3, Biobserve). Individual search strategy was classified by the observer as 'spatial' (straight to target or adjacent hole), 'serial' (several holes visited in a sequential manner before reaching the target), or 'random' (not spatial nor serial). Mice 'failed' if the target was not located within 3 min.

Open-field test

Mice were placed in the middle of the 44 × 64 cm arena delimited by opaque walls, and allowed to explore for 10 min. Distance travelled and time spent in the centre zone (20 × 36 cm) versus surrounding periphery were recorded by automated video tracking. After each test, mice returned to their home cages, and the arena was thoroughly cleaned with 70% ethanol.

Antibodies

We used primary antibodies against Akt (9272, 1:1000; Cell Signaling Technology, CST), P-Akt (Ser473) (4058, 1:1000; CST), CREB (06-863, 1:1000; Millipore), P-CREB (Ser133) (06-519, 1:500; Millipore), drebrin (ab12350, 1:1000; Abcam), ERK (p44/42 MAPK) (4696, 1:1000; CST), P-ERK (P-p44/42 MAPK) (Thr202/Tyr204) (9106, 1:1000; CST), GAPDH (sc-20357, 1:1000; Santa Cruz Biotechnology), GFAP (Z0334, 1:2000; Dako), Iba1 (019–19741, 1:1000; Wako), IGF1Rβ (3027, 1:1000; CST), IRβ (sc-711, 1:1000; Santa Cruz Biotechnology), neurofilament medium polypeptide (NEFM) (ab64300, 1:1000; Abcam), NeuN (MAB377, 1:1000; Millipore), synapsin I (AB1543P, 1:1000; Millipore), S6 ribosomal protein (2317, 1:1000; CST), and P-S6 ribosomal protein (Ser235/236) (4858, 1:1000; CST). Secondary antibodies were Alexa Fluor® 488 anti-mouse antibody (A11001, 1:1000; Life Technologies), biotinylated anti-rabbit antibody (BA-1000, 1:200; Vector Laboratories), horseradish peroxidase (HRP)-conjugated anti-rabbit antibody (656120, 1:500; Life Technologies), HRP-conjugated anti-mouse antibody (626520, 1:500; Life technologies), and IRDye-conjugated anti-mouse (925-32210, 1:20 000; LI-COR) and anti-rabbit (926-68021, 1:20 000; LI-COR) antibodies.

Histology and immunohistochemistry

Mice were transcardially perfused with PBS 0.1 M followed by 4% paraformaldehyde (PFA) at 4°C under deep pentobarbital anaesthesia. Brains were incubated in 4% PFA overnight at 4°C, transferred to 30% sucrose for 48 h, and frozen in isopentane at −40°C. Serial coronal sections (30 µm) were chosen to include the lateral ventricle. Sections were stained with 1% cresyl violet (C-5042, Sigma-Aldrich), or immunolabelled using specific antibodies and diamino-benzidine (K3468, Dako) reaction. Sections were incubated overnight with primary antibody at 4°C, and then incubated for 1 h at room temperature with secondary antibody. Images were acquired using a DM5000B microscope (Leica) and analysed using ImageJ software (National Institutes of Health).

Morphology of neurons and microglia

We analysed neuronal morphology as described (Gontier *et al.*, 2015). In brief, nucleus and soma size were determined by manually tracing the circumference of each NeuN-positive nucleus and each cresyl violet-stained neuronal soma using ImageJ. Four cortical brain sections (30-µm thick) per mouse were analysed. On average, 100 neurons of motor cortex layer V were measured per animal. To evaluate microglial morphology, we used four Iba1-stained sections per mouse (n = 4–6 mice/group). Total length per microglia was determined in motor cortex using AnalyzeSkeleton (ImageJ) (Leinenga and Götz, 2015).

Western blot

Mice were transcardially perfused with cold PBS under deep pentobarbital anaesthesia. Cortex and hippocampus were quickly dissected on ice and snap-frozen in isopentane. Brain tissue was homogenized in RIPA buffer (50 mM Tris, 150 mM NaCl, 1 mM EDTA, 1 mM EGTA, 1% Triton™ X-100, 0.1% SDS, 0.5% sodium deoxycholate) containing phosphatase inhibitors (10 mM NaF, 1 mM $NaVO_3$) and protease inhibitors (Roche) using a Polytron (Kinematica). Homogenates were centrifuged at 14 000 rpm for 20 min at 4°C. Supernatants were collected, and protein concentration determined using DC protein assay (Bio-Rad). For SDS-PAGE, 15, 40 or 60 µg of protein were electrophoresed through 4–20% gradient tris-glycine gels (Bio-Rad) and transferred onto polyvinylidene fluoride (PVDF) membranes. PVDF membranes were blocked for 1 h at room temperature with 5% non-fat dry milk in Tris-buffered saline containing 0.1% Tween 20. Membranes were incubated overnight at 4°C with primary antibodies followed by HRP- or IRDye-conjugated secondary antibodies for 1 h at room temperature. Blots were scanned using Odyssey CLx

(LI-COR) or revealed with ECL (WP20005, Life Technologies) and bands visualized using ChemiDoc and Quantity One 4.2.1 (Bio-Rad). Digital scans of entire membranes are in the Supplementary material. All western blot experiments were performed at least twice. Signals were quantified using Image Lab software (Bio-Rad) or Image Studio (LI-COR), and were normalized to GAPDH or to total proteins determined from Ponceau S-stained membranes.

Amyloid-β ELISA

Amyloid-β42 and amyloid-β40 peptides were extracted from cortical tissue, separated into formic acid-treated insoluble and diethylamine (DEA)-soluble fractions, and quantified using human specific-ELISA (Invitrogen) as described (Dansokho *et al.*, 2016). Results in Fig. 1H–J are from females. Males (not shown) revealed slightly lower amyloid-β levels (Gontier *et al.*, 2015), but no difference between genotypes.

Transmission electron microscopy

Ten microlitres of amyloid-β aggregated solution were adsorbed onto 200-mesh carbon and Formvar-coated grids (CF200-Cu-50, Euromedex), and negatively stained with 2.5% uranyl acetate for 45 s. Grids were examined using an electron microscope (EM 912 OMEGA, Zeiss) at 80 kV, and images captured with a digital camera (2 k × 2 k side-mounted TEM CCD, Veleta).

Laser microdissection and RNA extraction

Brains from 6-month-old female mice were quickly dissected, snap-frozen in isopentane at −40°C and stored at −80°C until use. We collected 30 coronal sections of 50-µm thickness per animal using a freezing microtome. Frozen sections were mounted on PEN-membrane 1 mm glass slides (#415101-4401-600, Zeiss), fixed for 2 min at 4°C in 70% ethanol, and stained in 1% cresyl violet (C-5042, Sigma-Aldrich). Sections were then dehydrated in 50% (30 s), 70% (30 s) and 100% ethanol (1 min) at 4°C, and air-dried. All solutions and materials were RNase-free to prevent RNA degradation. Laser assisted-microdissection was performed using a P.A.L.M. MicroBeam system with RoboSoftware (Zeiss). Total RNA was extracted from microdissected hippocampal CA1 by RNeasy® Micro Kit (74004, Qiagen) according to manufacturer's instructions and eluted with 14 µl of RNase-free water. RNA concentrations were determined using NanoDrop 1000 (Thermo Scientific).

Microarray processing and data analysis

After validation of RNA quality using Agilent RNA6000 nano chips and Bioanalyzer 2100, we reverse transcribed 25 ng of total RNA using Ovation Pico WTA System V2 (NuGEN). The resulting double strand cDNA was used for amplification based on SPIA technology. After purification according to the NuGEN protocol, 5.2 µg of sense target DNA were fragmented and biotin-labelled using Encore Biotin Module kit (NuGEN). After control of fragmentation using Bioanalyzer 2100, cDNA was hybridized to GeneChip Mouse Transcriptome Assay (MTA) 1.0 (Affymetrix) at 45°C for 17 h. After overnight hybridization, chips were washed on fluidic station FS450 following Affymetrix protocols and scanned using GCS3000 7G. Scanned images were analysed using Expression Console software (Affymetrix) to obtain raw data and metrics for quality control. Observations of metrics and distributions of raw data revealed no experimental outlier. Data were normalized using robust multiarray averaging (RMA, Bioconductor software). We first controlled and analysed data by principal component analysis (PCA) and used one-way ANOVA to extract differentially expressed genes with Genomics Suite (Partek). We performed expression analysis to identify single genes, but also to discover differentially activated key cell functions. Enrichment analyses were performed using Ingenuity Pathway Analysis (IPA, Qiagen) and Pathway Studio (PWS, Insilicogen) software, with threshold fixed to $P < 0.02$.

Statistical analysis

Data are presented as mean ± standard error of the mean (SEM). Sample size for each experiment was estimated based on previous experiments using these models and/or pilot studies (Cohen *et al.*, 2009; Gontier *et al.*, 2015). Mice matched by gender, age, genotype and weight were randomly assigned to experimental groups. Investigators were blinded to group allocation (AβOs, genotype) during experiments, data collection and analysis. No mice were excluded from analysis except in behavioural studies based on the preset criterion: animal does not move during test. Statistical tests were performed using Prism (GraphPad). *F*-test was conducted to test normal distribution and homogeneity of variance. For normally distributed data, groups were compared using two-tailed unpaired Student's *t*-test or ANOVA. Otherwise we used Mann-Whitney U-test or Kruskal-Wallis test. Data from Barnes maze experiments were analysed by repeated measures (RM) two-way ANOVA and Fisher's exact test. $P \leqslant 0.05$ was considered significant. Microarray data were analysed by one-way ANOVA using a threshold of $P < 0.02$ to select differentially expressed genes.

Results

Inactivation of neuronal IGF signalling during advanced-stage Alzheimer's disease does not mitigate amyloid pathology

We previously showed that blocking adult neuronal IGF signalling during presymptomatic disease phase alleviates subsequent amyloid pathology and prevents cognitive deficits in APP/PS1 (AD) mice, mainly by favouring amyloid-β clearance (Gontier *et al.*, 2015). To gain further insight, also into the therapeutic potential of interfering with IGF signalling, we here asked whether disrupting IGF1R during symptomatic Alzheimer's disease stages could still affect a full-blown disease phenotype. We therefore knocked out IGF1R in CaMKIIα-positive forebrain neurons of old (age 17 month) APP/PS1 mice (a mutant that we called

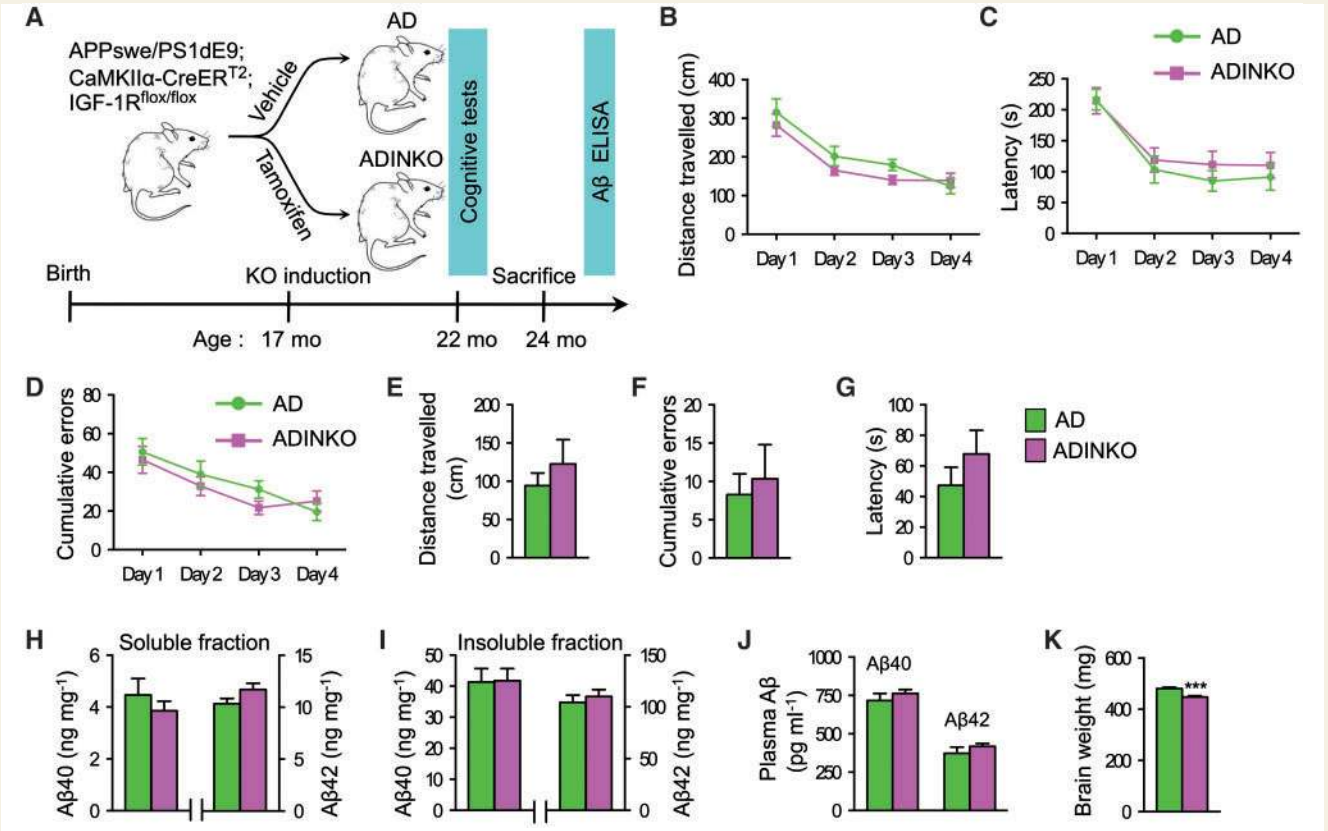

Figure 1 Blocking neuronal IGF signalling in old mice during advanced stages of Alzheimer's disease does no longer protect from amyloid pathology. (**A**) We induced neuronal IGF1R knockout at age 17 months by intraperitoneal tamoxifen injection in APPswe/PS1dE9;CaMKIIα-CreER^{T2};IGF1R$^{flox/flox}$ mice that exhibit late-stage amyloid pathology (ADINKO). Alzheimer's disease mice (AD) received vehicle and served as control. Mice were submitted to cognitive tests 5 months later and amyloid pathology evaluated thereafter. (**B–G**) Learning memory was assessed by training in a Barnes maze, four times per day for 4 days, and all groups of mice succeeded in learning (repeated measures ANOVA for time $P < 0.0001$) (**B–D**). Long-term memory retention was assessed on Day 5 (**E–G**). n = 15–20 mice. Males and females performed similarly and groups were combined. (**H** and **I**) Amyloid-β40 and amyloid-β42 abundance in cortical homogenates of old ADINKO and AD mice. Soluble (**H**) and insoluble fractions (**I**) were measured by human specific ELISA. n = 9–11 mice. (**J**) Plasma amyloid-β40 and amyloid-β42 were assayed in old ADINKO and AD mice. n = 9–11 mice. (**K**) Wet weight of ADINKO brain diminished. Mann-Whitney U-test, $^{***}P < 0.001$, n = 20 mice. Data are mean ± SEM.

ADINKO), when APP/PS1 mice exhibit advanced amyloid pathology and multiple Alzheimer's disease symptoms (Fig. 1A). To find out whether IGF1R suppression still improved Alzheimer's disease-related behavioural deficits, we analysed spatial memory using the Barnes maze 5 months later. Both ADINKO and AD mice succeeded in learning the maze through repeated training sessions, as evidenced by decreased distance travelled, shorter latency, and fewer cumulative errors over days (Fig. 1B–D). Similar to this unchanged learning ability, memory retention was also indistinguishable between ADINKO and AD mice (Fig. 1E–G). To directly assess the effects of IGF1R inactivation in old mice on advanced amyloid pathology, we measured cortical abundance of amyloid-β peptides in soluble and insoluble fractions. Again, and in clear contrast to receptor inactivation performed in young mice (Gontier *et al.*, 2015), we found that after inactivation at advanced age, cortical amyloid-β40 and amyloid-β42 levels were similarly elevated in ADINKO and AD mice (Fig. 1H and I), and the same was true for plasma amyloid-β40 and amyloid-β42 (Fig. 1J). These results indicated that suppressing neuronal IGF1R at advanced-stage Alzheimer's disease could not mitigate advanced brain amyloid pathology, nor did it improve systemic amyloid-β clearance. Yet, our neuron-specific IGF1R knockout induced at old age was not lacking efficiency: Cre-lox gene excision was as wide-spread as in brains induced in young mice, and loss of IGF1R led to the same marked changes in cell homeostasis and typical reduction in neuronal soma size, that were also evidenced by slightly, but significantly diminished brain weight (Fig. 1K; −7%, $P < 0.0001$) and reduced cerebral cortical mass (hemi-cortex: ADINKO 72.1 ± 1.5 mg versus AD 87.4 ± 1.2 mg, n = 20–21, −17%, $P < 0.0001$).

To selectively address the predicted neuroprotective effects of neuronal IGF1R knockout induced in old brains, we switched to an *in vivo* mouse model of acute amyloid-β

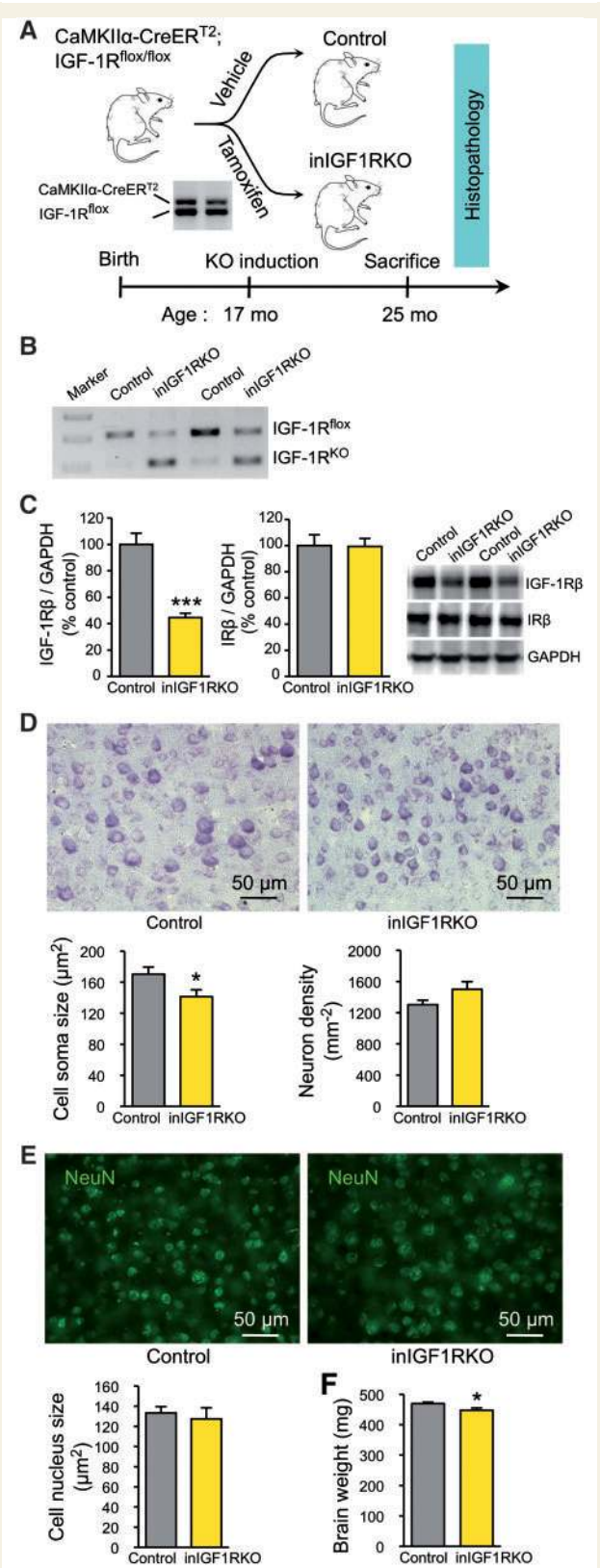

Figure 2 Deleting IGF1R from aged neurons entails histomorphological changes in the forebrain. (**A**) Inducible neuron-specific IGF1R knockout (inIGF1RKO) was achieved combining CaMKIIα-CreER^{T2} transgene with floxed *Igf1r* alleles (IGF1R$^{flox/flox}$). CaMKIIα-CreER^{T2};IGF1R$^{flox/flox}$ mice were intraperitoneally injected with tamoxifen at age 17 month; controls received vehicle alone. (**B**) Gene deletion (IGF1R^{KO}) monitored by PCR in hippocampus (n = 10–12 mice per group). (**C**) Western blot analysis of hippocampus. Mann-Whitney U-test, ***$P < 0.001$, n = 10 mice per group. (**D**) Representative micrographs of cresyl violet-stained cortical neurons. Neuronal soma size was reduced in inIGF1RKO cortex while neuron density remained unchanged. Two-tailed unpaired Student's t-test, *$P \leq 0.05$, n = 7–8 mice per group. Four brain sections were analysed per mouse. (**E**) Cell nucleus size was measured from NeuN-stained sections, n = 10–12 mice per group. (**F**) Wet weight of inIGF1RKO and control brain. Mann-Whitney U-test, *$P \leq 0.05$, n = 7 mice per group. Bar graphs represent mean ± SEM.

proteotoxicity, consisting of AβO intracerebroventricular injection in mice with inducible neuronal IGF1R knockout (inIGF1RKO). Inducing IGF1R knockout alone at old age produced efficient hippocampal Cre-lox excision of floxed IGF1R alleles (Fig. 2A and B) and a marked (55%) local decrease in IGF1R protein ($P < 0.001$), while insulin receptor levels remained unchanged (Fig. 2C). In accordance with the relative proportion of neurons versus other cell types (Herculano-Houzel *et al.*, 2006), results indicated that IGF1R was ablated in almost all CaMKIIα-positive hippocampal neurons. We reported that neuronal IGF1R knockout at young age reduced neuronal soma size in an Alzheimer's disease context (Gontier *et al.*, 2015). Here we showed that IGF1R ablation in old mice similarly leads to significant decrease in neuronal soma size (−17%, $P < 0.05$), while neuron density and cell nucleus size remained unchanged (Fig. 2D and E). Diminished neuronal cytoplasm also provoked reduced brain weight in inIGF1RKO mice (Fig. 2F; −5%, $P < 0.05$), demonstrating that IGF signalling exerts robust and lifelong control of soma size in post-mitotic neurons.

Neuronal IGF1R knockout in old mice alleviates cognitive deficits induced by amyloid-β oligomers

AβOs are considered key mediators of synaptic and cognitive impairments in Alzheimer's disease (Lesné *et al.*, 2013; Ferreira *et al.*, 2015). Intracerebroventricular injection of AβOs has been successfully used as proteotoxic insult causing neuronal dysfunction, synapse failure, cell metabolic and cognitive dysfunctions (Clarke *et al.*, 2015). We generated AβOs by *in vitro* aggregation and checked quality by transmission electron microscopy. Amyloid-β incubation for 48 h at 37°C yielded a homogeneous product of 10–30 nm AβOs (Supplementary Fig. 1). This product was intracerebroventricularly injected into the brains of old inIGF1RKO and control mice in which the knockout had been induced several months earlier (Fig. 3A). To find out whether inactivation of IGF signalling protected from AβO-induced spatial memory deficits, we tested the mice in a Barnes maze. Time to reach the refuge box ($P < 0.0001$),

number of errors ($P < 0.01$), and distance travelled ($P < 0.001$) were significantly reduced over days in all groups, indicating effective learning in the absence of IGF1R and/or after AβO challenge (Fig. 3B). However, during the memory-retention test, AβO-treated mice searched twice as long for the refuge box than control mice (Fig. 3C; $P < 0.05$), revealing AβO-induced long-term spatial memory deficits. Importantly, these deficits were no longer observed in inIGF1RKO + AβO mice. The better memory performance of inIGF1RKO + AβO mice compared with AβO mice was all the more evident since they preferentially used a spatial search strategy (Fig. 3D) (AβO, 33%; inIGF1RKO + AβO, 67%; Fisher's exact test, $P < 0.001$). In addition, more AβO-treated mice failed the memory-retention test than control mice (failure: control 20%; AβO 48%; Fisher's exact test, $P < 0.001$), and we observed a rescue of the proteotoxic phenotype in inIGF1RKO + AβO mice compared with AβO mice (Fig. 3D) (failure: inIGF1RKO + AβO 10%; Fisher's exact test, $P < 0.001$). Besides memory impairments, Alzheimer's disease also involves anxiety and sensory motor perturbations, which can be assessed by the open-field test. Results revealed no difference in speed and distance travelled between groups (data not shown), suggesting AβOs

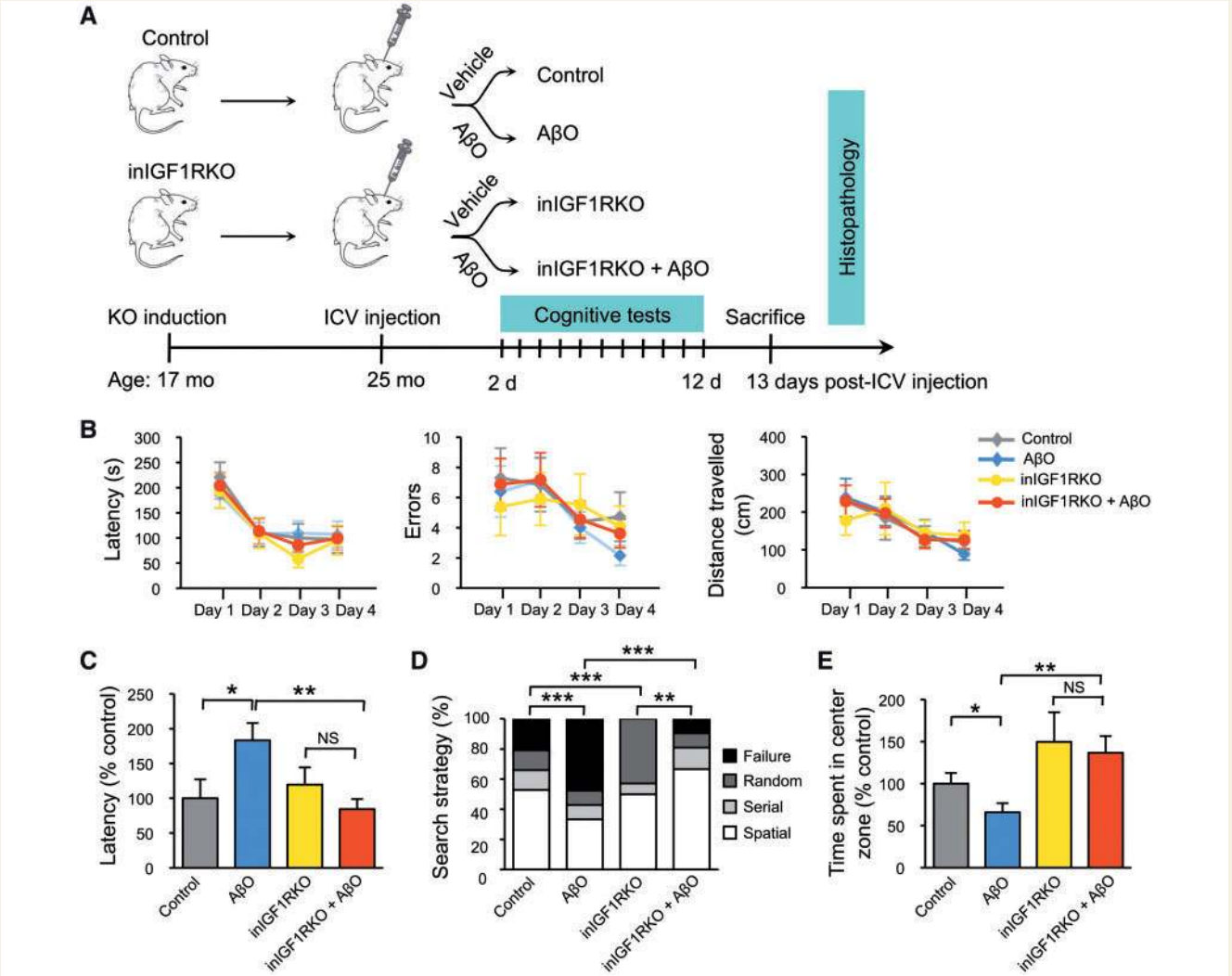

Figure 3 Suppression of neuronal IGF1R in aged mice prevents amyloid-β oligomers-induced cognitive deficits. (**A**) Control and inIGF1RKO mice, tamoxifen-induced at age 17 months, were injected intracerebroventricular with AβOs or vehicle at age 25 months. Behaviour was subsequently tested in Barnes maze and open-field. (**B**) Control and inIGF1RKO mice started training 72 h after AβO injection in a Barnes maze, four times per day for 4 days. In all groups, latency ($P < 0.0001$), errors ($P = 0.01$) and distance travelled ($P < 0.001$) diminished, indicating effective learning. Ability to learn remained unaffected by suppression of IGF1R and/or administration of AβOs (repeated measures ANOVA). (**C** and **D**) Reference memory was tested 24 h after the last training. Latency (**C**) doubled in AβO-injected controls and normalized in the absence of neuronal IGF1R (Mann-Whitney U-test, $^*P \leqslant 0.05$, $^{**}P < 0.01$). Similarly, failure in AβO-injected controls to find the target hole was rescued in inIGF1RKO mice (**D**) (Fisher's exact test, $P < 0.001$). n = 14–21 mice per group. (**E**) Open-field test on Day 11 post-intracerebroventricular injection revealed decreased anxiety-like behaviour of inIGF1RKO mice (Mann-Whitney U-test, $^*P \leqslant 0.05$, $^{**}P < 0.01$), n = 14–20 mice per group. Data are mean ± SEM.

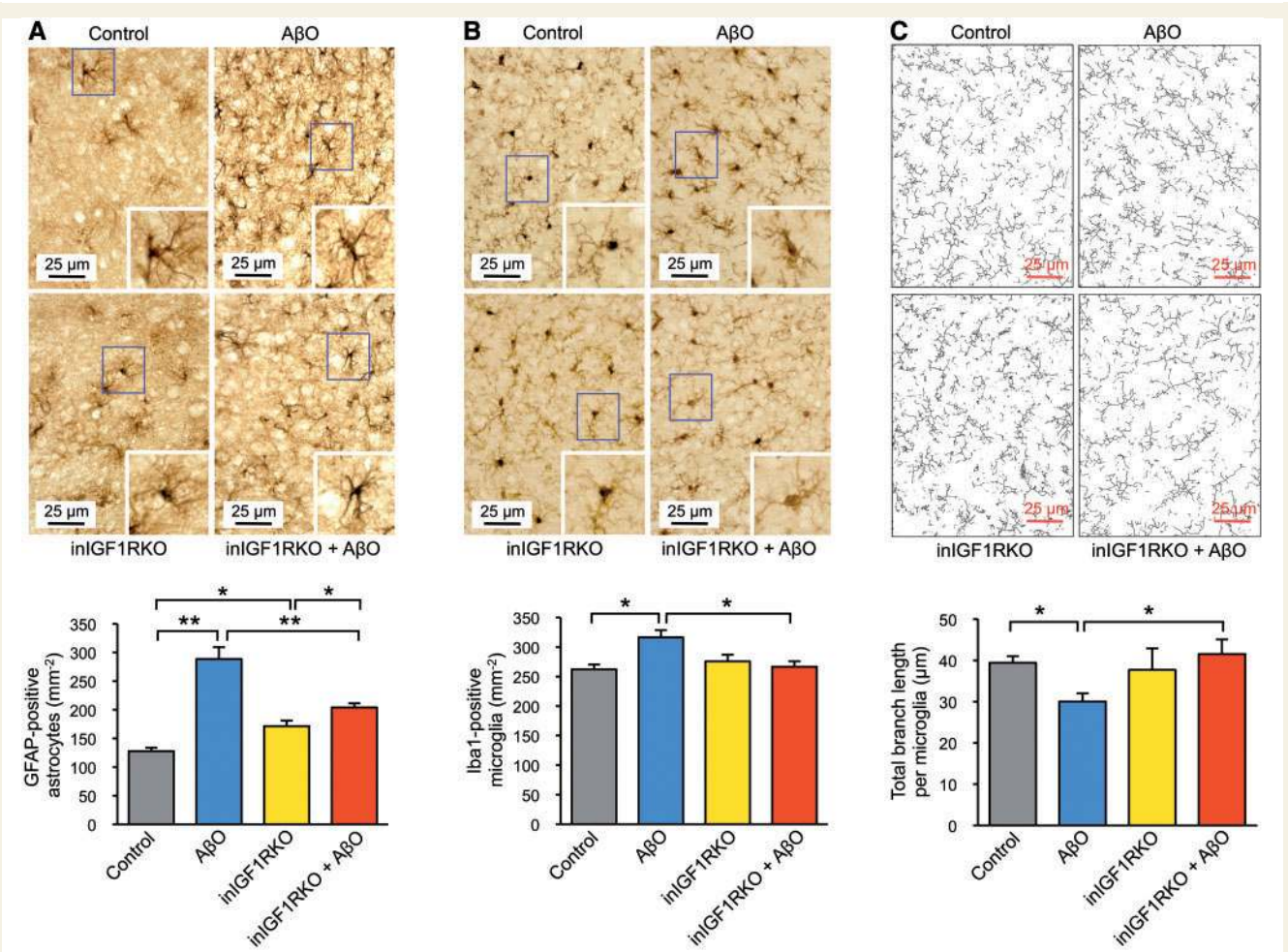

Figure 4 inIGF1RKO brains are protected from AβO-induced reactive neuroinflammation. Immunohistochemistry was performed 13 days after intracerebroventricular injection. (**A**) Density of astrocytes in cortex was determined from GFAP immunostaining. (**B**) Anti-Iba1 IHC revealed that density of microglia was normalized in cortex of inIGF1RKO mice. (**C**) Total branch length per microglia was determined using AnalyzeSkeleton (ImageJ). Mann-Whitney U-test, $*P \leqslant 0.05$, $**P < 0.01$, $n = 4$–6 mice per group; four brain sections were analysed per mouse. Data are mean ± SEM.

did not induce motor deficits. After a single intracerebroventricular injection of AβOs, mice avoided the anxiogenic centre (Fig. 3E; −34%, $P < 0.05$). In contrast, the behavioural pattern of inIGF1RKO mice remained unaffected by AβO injection, indicating that blocking neuronal IGF1R protected against AβO-induced anxiety. Collectively, behavioural data demonstrated that IGF1R suppression in old mice, prior to AβO proteotoxic challenge protected from cognitive and anxiety-like defects.

Blocking neuronal IGF signalling alleviates amyloid-β oligomer-associated inflammation

Intracerebroventricular-injected AβOs reliably induce brain inflammation (Choi and Bosetti, 2009; Clarke *et al.*, 2015). We therefore asked whether the rescue in cognitive functions was accompanied by improved inflammatory status. In control mice, AβO administration resulted in a robust astrogliosis, with a >2-fold increase in density of cortical astrocytes (Fig. 4A; $P < 0.01$). In contrast, the AβO-induced increase in astrocyte density was limited to 19% in inIGF1RKO mice ($P < 0.05$). Thus, AβOs provoked significantly less astrogliosis in inIGF1RKO cortex than in controls ($P < 0.01$). AβOs also caused a 21% increase in density of Iba1-positive microglia in control mice, but failed to induce microgliosis in inIGF1RKO mice (Fig. 4B; $P < 0.05$). Depending on activation, morphology of microglia ranges from highly ramified to amoeboid-like. To explore microglia activation, we quantified branching. Total branch length per microglia was significantly reduced in AβO-injected controls (−24%, $P < 0.05$; Fig. 4C), which is typical of enhanced activation (Liaury *et al.*, 2012; Andreasson *et al.*, 2016), whereas microglia in inIGF1RKO + AβO mice was similar in phenotype to control and inIGF1RKO mice (Fig. 4C; $P < 0.05$). Thus, while

microglia in AβO mice were strongly activated, they appeared less reactive in inIGF1RKO + AβO mice, suggesting that neuroinflammatory response was limited, most likely due to more efficient elimination of toxic peptides in inIGF1RKO + AβO brains. We also tried to evidence AβO-induced damage at the synaptic level by measuring drebrin and synapsin. However, we found no changes in synaptic proteins, possibly because 2 weeks after the proteotoxic challenge, and following multiple behavioural tasks, synapses had mostly recovered (Supplementary Fig. 2). Together, these results strongly indicated that neuronal IGF1R knockout induced in old mice protected against AβO-induced neuroinflammation.

Neurons in early-stage Alzheimer's disease and IGF1R knockout neurons exhibit convergent transcriptomic signatures

To explore the gene expression signature that protects IGF1R knockout neurons from amyloid-β proteotoxicity, we performed a genome-wide microarray analysis of microdissected CA1 from young control, inIGF1RKO, AD and ADINKO mice (Fig. 5A). We chose the hippocampal CA1 because of its compact population of pyramidal neurons (Supplementary Fig. 3), and its known vulnerability to degeneration (Ginsberg *et al.*, 2012; Landel *et al.*, 2014). Overall gene expression levels among the four groups were the same, as evidenced by principal component analysis and normalized intensities of all probes (Supplementary Fig. 4). The highest number of differentially expressed genes was observed when comparing inIGF1RKO mice with controls, revealing 623 up- and 513 downregulated genes. Comparing ADINKO with AD mice, we identified 178 up- and 107 downregulated genes (Fig. 5B). The proportion of molecular categories encoded by differentially expressed genes were conserved between experimental groups and include predominantly enzymes, transcription regulators, transporters, and G protein-coupled receptors (Supplementary Fig. 5). The top five altered gene networks for each pairwise comparison highlighted functional annotations mostly related to nervous system and neurodegenerative diseases, reflective of the homogenous population of CA1 pyramidal neurons (Supplementary Fig. 6). We next analysed effects of Alzheimer's disease on neuronal integrated functions using PWS software, and found that Alzheimer's disease-regulated genes involved in six main cell functions, namely neurotransmission, neuronal growth and differentiation, signal transduction, metabolism, stress response and proteostasis (Fig. 5C and Supplementary Table 1). Consistently, Alzheimer's disease also affected these same functions in IGF1R knockout neurons (Supplementary Fig. 7A, Supplementary Tables 2 and 3). Interestingly, neuronal IGF1R deletion impacted essentially the same six main cell functions (Fig. 5D and Supplementary Table 4). Using IPA, we confirmed that early stage Alzheimer's disease and neuronal IGF1R ablation affected strongly overlapping biological pathways (Supplementary Fig. 7B–F, Supplementary Tables 5 and 6). Within these integrated neuronal functions, Alzheimer's disease and IGF1R deletion affected 29 biological processes, of which 25 changed in the same direction: these processes mainly involved cytoskeleton organization, neurite growth, differentiation, cellular stress response and synaptic transmission (Fig. 5E). Moreover, our analysis revealed that 102 of 103 changes in gene expression common to Alzheimer's disease and IGF1R ablation occurred in the same direction, only the expression of neurofilament medium polypeptide *Nefm* changed in the opposite direction (Fig. 5F and G). Overall, these results clearly indicated that transcriptomic signatures of neurons from AD and inIGF1RKO mice exhibit strong and extended similarities. These findings suggest that early stage Alzheimer's disease neurons activate a neuroprotective program resulting in cellular changes very similar to those occurring after specifically neuronal IGF1R ablation. Note that when we extracted all transcription factors with significantly altered gene expression from the microarray data (Supplementary Table 7), filtering them for known implication in Alzheimer's disease pathogenesis and comparing AD with inIGF1RKO groups, we obtained several candidate transcriptional regulators, including *Arntl*, *Ezh2*, *Hdac5* and *Xbp1*, which all behaved identically in both groups. It is likely that these transcription factors contributed to the similitude of AD and inIGF1RKO neuronal behaviour.

IGF1R suppression in adult Alzheimer's disease neurons reverses specific cell functions

By comparing the transcriptome signatures of ADINKO with AD neurons using PWS software, we found that IGF1R deletion primarily regulated genes involved in signal transduction, stress response, neurotransmission, growth and differentiation (Fig. 6A and Supplementary Table 8). Interestingly, neuronal IGF1R inactivation affected markedly fewer biological functions in AD neurons than in control neurons (*cf.* Fig. 6A and Fig. 5D). Consistent with that result, we obtained similar results using IPA (Supplementary Fig. 7, Supplementary Tables 9 and 10). Changes in gene expression common to AD and to ADINKO neurons impacted essentially six major cell biological processes, of which five were regulated in the opposite direction (Fig. 6B). This was closely linked to the fact that 52 of 53 gene changes common to AD and ADINKO neurons were reversed (Fig. 6C and D). Genes with significantly altered expression included several that are known to be affected by Alzheimer's disease, namely transthyretin (*Ttr*), 24-dehydrocholesterol reductase (*Dhcr24*), and the membrane G protein-coupled receptor kinase 5 (*Grk5*). Of note, *Nefm* was one of the three genes that were differentially regulated in all comparisons

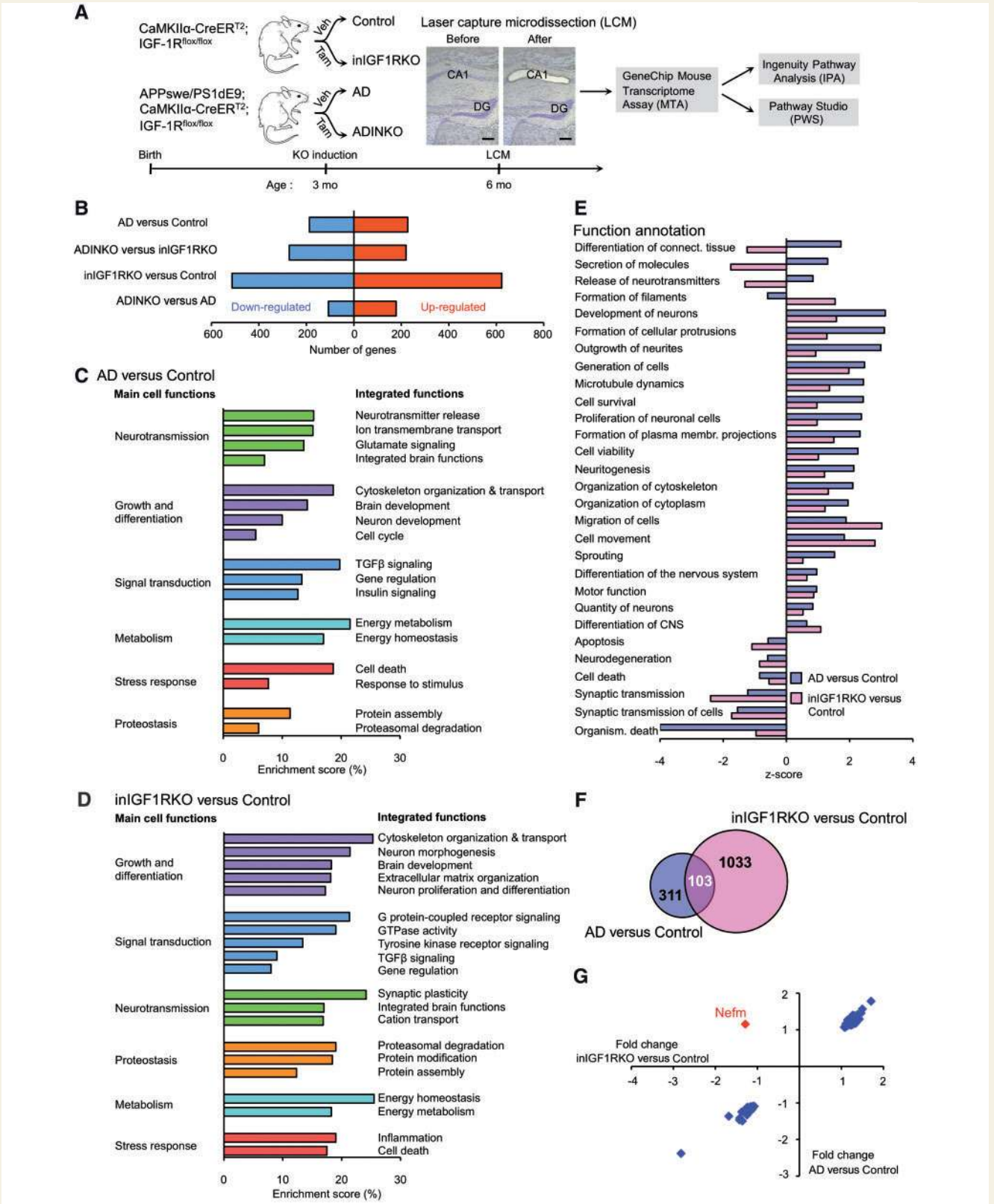

Figure 5 Transcriptional signatures of neurons from early-stage Alzheimer's disease and of neurons with adult-onset IGF1R knockout reveal similar pattern of affected biological pathways and share many differentially expressed genes. (**A**) CaMKIIα-CreER^{T2};IGF1R$^{flox/flox}$ and APPswe/PS1dE9;CaMKIIα-CreER^{T2};IGF1R$^{flox/flox}$ mice were intraperitoneally injected with tamoxifen or with vehicle alone at 3 months of age. Hippocampus CA1 was laser-microdissected from brain sections of 6-month-old control, inIGF1RKO, AD and ADINKO mice. We used GeneChip Mouse Transcriptome Assay (MTA) for genome-wide microarray, and performed functional analyses by Pathway Studio (PWS) and Ingenuity Pathway Analysis (IPA) software. Scale bar = 600 μm. (**B**) Number of significantly (i.e. $P < 0.02$) up- (red) or downregulated

(continued)

(Supplementary Fig. 8C and D). Consequently, 12.6% (52 of 414) of all genes deregulated in AD were significantly reversed in ADINKO mice. Taken together, these data clearly demonstrated that a conspicuous number of Alzheimer's disease-associated transcriptional and functional changes are counteracted by preceding neuronal IGF1R deletion. Neurons knockout for IGF1R that subsequently develop Alzheimer's disease show restrained expression of a significant number of genes that are all involved in the endogenous reaction of neurons to amyloid-β proteotoxicity. This appears as a coordinated prevention of gene overexpression entailing benefits in case of neurodegenerative disease. The limitation of inflammatory response, previously demonstrated in ADINKO mutants, may be a typical example for these beneficial effects. Finally, we used differentially expressed genes common to both comparisons to assemble a gene network depicting intramodular connections and hub genes (Fig. 6E). This molecular network clustered around key genes coding for Akt (Ak murine thymoma proto-oncogene protein family), APP (amyloid precursor protein), CREB1 (cAMP responsive element binding protein 1), HSPA8 (heat shock 70 kDa protein 8), and UBC (ubiquitin C). Significantly, biological functions represented by this network included amino acid and lipid metabolism, cell morphology, synaptic transmission, dementia and learning (Supplementary Table 11). We next selected key elements of this network and investigated how their differential expression translated into protein. For this, we used hippocampi at 6 and 17 months of age in which IGF1R had been deleted at 3 months. Similar to the findings in old mice (Fig. 2D), ablation of IGF1R at 3 months led to swift reduction of neuronal soma size in inIGF1RKO and in ADINKO mice (Fig. 7A). Through IPA and PWS analysis, we had identified cytoskeleton organization as an integrated function that was significantly impacted by Alzheimer's disease and IGF1R deletion (Supplementary Tables 1 and 4–6). Here, we focused on NEFM. At 6 months, hippocampal NEFM was diminished in inIGF1RKO and ADINKO (Fig. 7B). At 17 months, when major Alzheimer's disease symptoms were present, neuropathology markedly increased NEFM levels, while ablation of neuronal IGF1R reduced NEFM levels, in inIGF1RKO and in ADINKO brains. Thus, complete suppression of neuronal IGF signalling in AD mice restored hippocampal NEFM to control levels. Network analysis (Fig. 6E) suggested that Akt and CREB could play key roles in regulating interactions. Since Akt and CREB were not differentially expressed, we explored their hippocampal phospho-activation. We also examined phosphorylation of ERK1/2, a canonical pathway involved in IGF signalling, and S6 ribosomal protein (S6) that functions downstream of Akt. Total levels of Akt, ERK1/2, S6 and CREB were not changed among the four experimental groups. However, P-Akt (Ser473), P-ERK1/2 (Thr202/Tyr204) and P-S6 (Ser235/236) were increased in AD mice (two-way ANOVA, effect of AD: $P < 0.001$, Fig. 7C). This increase was 2- to 4-fold in P-Akt, P-S6 and P-ERK1/2. IGF1R deletion tended to reduce phospho-activation of Akt, S6 and ERK1/2 comparing ADINKO with AD mice, though this did not reach statistical significance (for P-S6, ADINKO versus AD: $P = 0.09$, Fig. 7C). By contrast, P-CREB (Ser133) increased in the absence of IGF1R, both in physiological and pathological context, while Alzheimer's disease had no effect on P-CREB (Fig. 7C). Together, this suggested differential roles for Akt pathways and CREB in the interactions between IGF signalling and Alzheimer's disease. Interestingly, at 17 months, the situation had again much evolved and we observed strong effects of Alzheimer's disease, namely conspicuous decrease in P-Akt and P-S6 (two-way ANOVA, effect of AD: $P < 0.0001$, Fig. 7D). Taken together, gene network analysis clearly identified several key factors linking inactivation of IGF signalling to functions determining resistance to neurodegeneration.

Discussion

Neuronal IGF1R blockade promotes long-term neuroprotection against amyloid-β proteotoxicity

Our results demonstrate that IGF1R-deficient neurons are more resistant to AβO proteotoxicity, as evidenced by improved behavioural outcome and diminished neuroinflammation. This resistance to proteotoxicity developed regardless of amyloid plaques, extending on the recent discovery of nerve cell-specific neuroprotective and anti-degenerative mechanisms controlled by IGF signals (Biondi *et al.*, 2015; De Magalhaes Filho *et al.*, 2017). Interestingly, ablating IGF1R in neurons of old mice could not mitigate amyloid-β load during advanced amyloid pathology in AD mice, but conferred neuroprotection against AβO toxicity.

Figure 5 Continued

(blue) genes in all four pairwise comparisons. (**C** and **D**) All significantly affected integrated functions were identified using PWS and ranked, with the most affected on top. Altered integrated functions in AD neurons (**C**) and inIGF1RKO neurons (**D**) compared with controls. (**E**) IPA revealed that 25 of 29 neuronal biological processes affected in both AD neurons and inIGF1RKO neurons were altered in the same direction. (**F**) Venn diagram representing the numbers of differentially expressed genes from AD mice versus control comparison and from inIGF1RKO mice versus control comparison, and their overlap. (**G**) Of 103 significant changes in gene expression common to AD and inIGF1RKO, 102 occurred in the same direction (blue). Solely the neurofilament medium polypeptide *Nefm* was significantly regulated in the opposite direction (red). One-way ANOVA, $P < 0.02$, $n = 5$ mice per group.

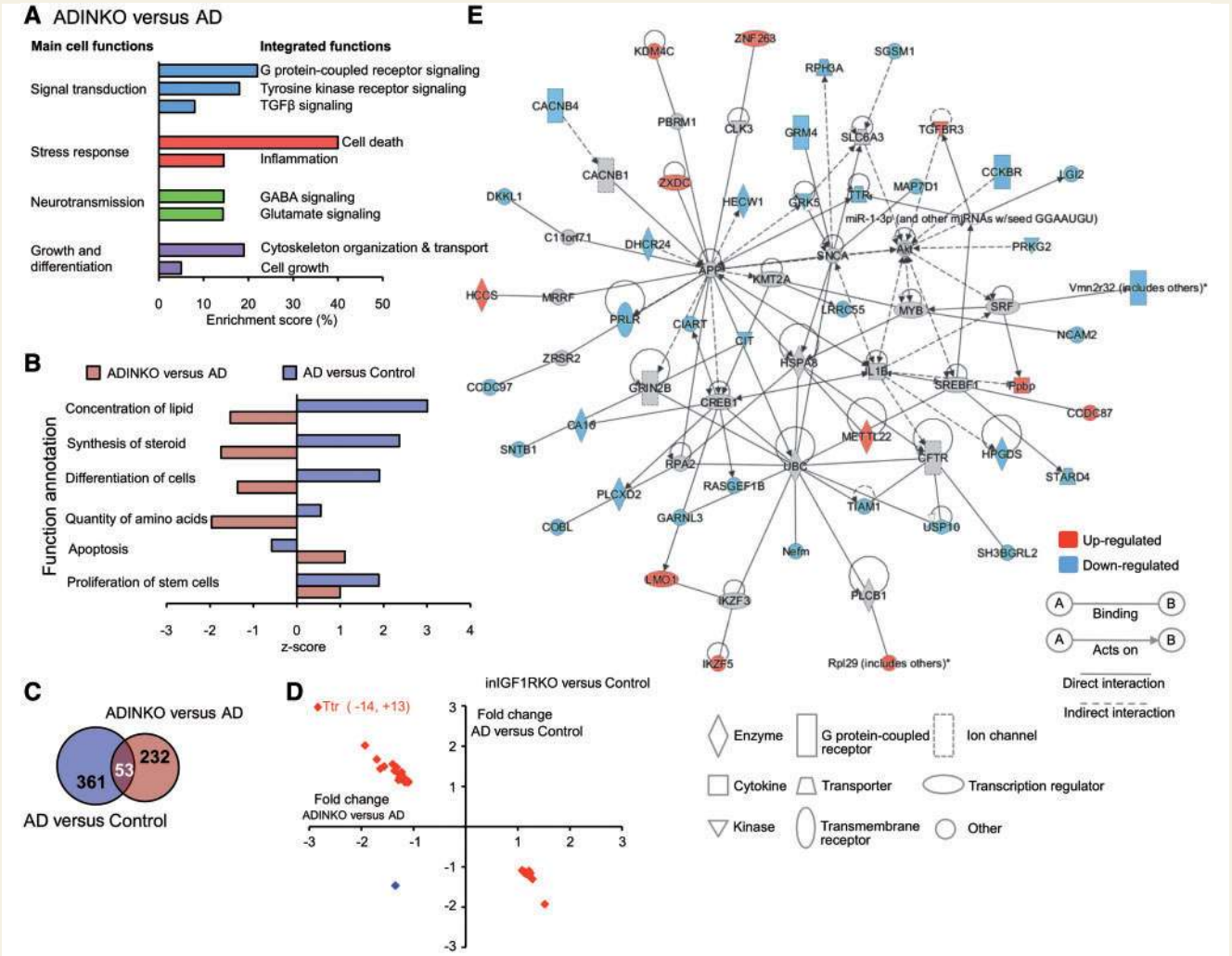

Figure 6 Blocking IGF signalling in AD neurons reverses biological networks involved in lipid and amino acid metabolism, cellular stress response and proteostasis. (**A**) Integrated functions that are significantly impacted in ADINKO neurons compared with AD neurons, identified using PWS. (**B**) IPA revealed that five of six neurobiological processes affected in both AD and ADINKO neurons were reversed in the latter. (**C**) Venn diagram representing the number of differentially expressed genes affected in AD versus control comparison and in ADINKO versus AD comparison. (**D**) Of 53 gene expression-changes common to AD and ADINKO neurons, 52 were reversed in the latter (red). Additional Venn analyses are in Supplementary Fig. 8. (**E**) Transcriptome network integrating 43 of 53 differentially expressed genes identified in both AD versus control and ADINKO versus AD comparison. Overlay was from ADINKO versus AD comparison. Main clusters were genes coding for Akt, APP, CREB1, UBC and HSPA8. IPA, one-way ANOVA, $P < 0.02$, $n = 5$ mice per group.

These data imply that neuroprotective mechanisms are effective before irreversible Alzheimer's disease-related brain damage occurred and cognitive decline started. While this clearly suggested a significant potential to prevent Alzheimer's disease, more research is needed to understand why these neuroprotective mechanisms are less efficient in advanced stages of the disease. Importantly, we demonstrated that ablating IGF signalling in aged neurons renders the mammalian brain resistant to acute insult by AβOs and that this effect is not temporally restricted. Our findings in mice are in line with recent work in nematodes indicating insulin/IGF1 signalling (IIS) inhibits axon regeneration in aged motor neurons (Byrne *et al.*, 2014). Whereas IGF signalling controls lifespan across species, our data demonstrated in a mammalian species that neuronal IGF signalling regulates long-term neuroprotective capacities, most likely in a cell-autonomous manner

Alzheimer's disease neurons and IGF1R-ablated neurons share extended transcriptomic characteristics

Our study is the first to report on the transcriptional signature of adult-onset IGF1R-deficient neurons in physiological and Alzheimer's disease conditions. At the chosen time of analysis (age 6 months), Alzheimer's pathology in

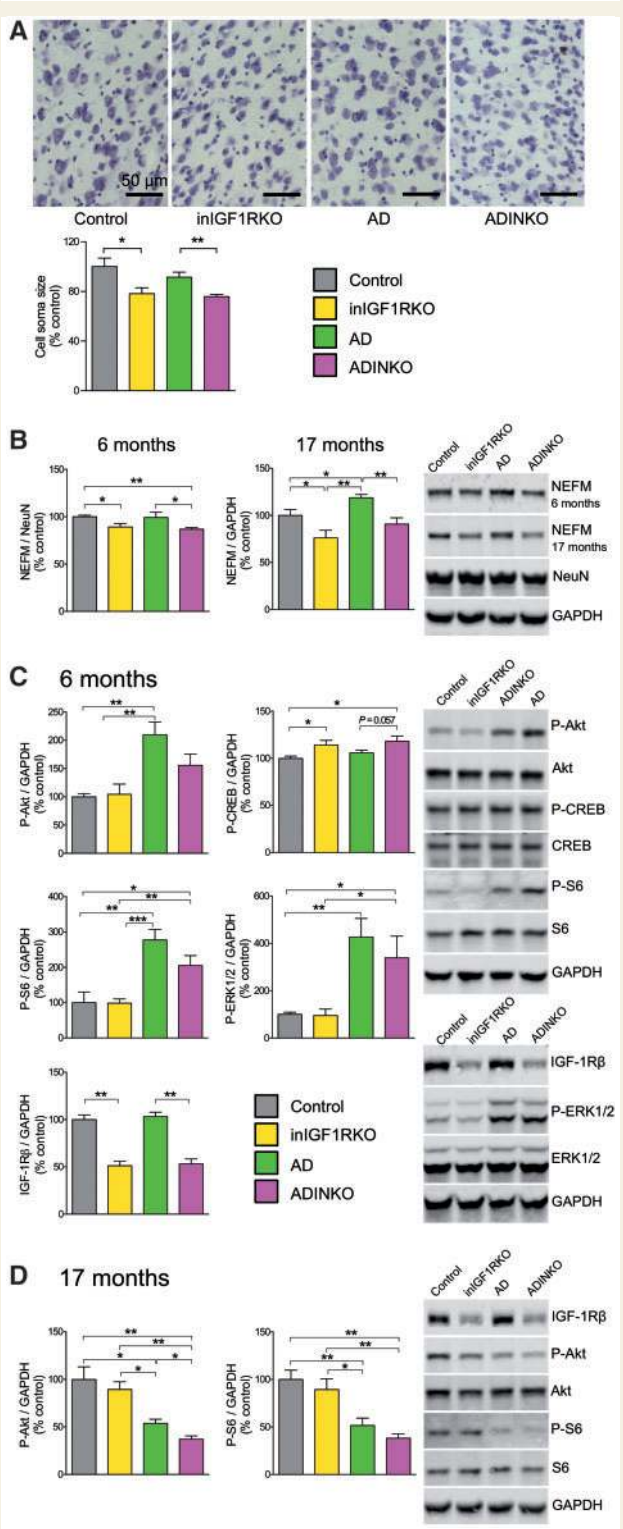

Figure 7 Neuronal cell size, cytoskeleton organization and signal transduction affected by IGF1R knockout and Alzheimer's disease. (**A**) Size of cell soma in cortical neurons from 6-month-old mice. Representative brain sections and morphometric quantification. Mann-Whitney U-test, $*P \leqslant 0.05$, $**P < 0.01$, $n = 5$–6 mice per group. (**B**) Western blot of NEFM in hippocampus relative to NeuN, at 6 and 17 months of age. GAPDH served as loading control. (**C**) Western blot of P-Akt, P-S6, total P-ERK, P-CREB and IGF1R, together with representative scans from immunoblots, all at age 6 months. Note that the order of groups in scans differs between panels. (**D**) Western blot of P-Akt and P-S6 in 17-month-old hippocampus. Two-way ANOVA was used to test IGF1R knockout or Alzheimer's disease effect, followed by Mann-Whitney U-test; $*P \leqslant 0.05$, $**P < 0.01$, $***P < 0.001$, $n = 5$–7 mice per group. Data are mean ± SEM.

APP/PS1 mice is under way but plaques are still rare and neuroinflammation limited (Jankowsky *et al.*, 2004), allowing us to record the early adaptive response to amyloid-β accumulation in CA1 neurons. Microarray analysis revealed that the biological functions principally associated with neuronal IGF1R ablation are much the same as those altered by Alzheimer's disease, namely neurotransmission, growth and differentiation, signal transduction, cellular stress response, metabolism and proteostasis. Moreover, the genes differentially regulated by Alzheimer's disease and by IGF1R deletion were almost all regulated in the same direction. The functions associated with these differentially expressed genes pertained specifically to neurite growth, cytoskeleton organization, differentiation, cellular stress response and synaptic transmission. We hypothesized that Alzheimer's disease neurons activate a set of protective molecular pathways, aiming at similar targets as IGF1R-deficient neurons, in an attempt to fight amyloid pathology during the early disease phase. This defence mechanism, however, failed in the course of the disease leading to accumulation of amyloid-β aggregates during ageing. Several laboratories reported hyperactivity of mTOR in post-mortem human Alzheimer's disease brains, mTOR belonging to the PI3K-Akt pathway downstream of IGF1R (Talbot *et al.*, 2012; Tramutola *et al.*, 2015). Less data are available on related kinases such as S6 ribosomal protein and Akt. Our findings indicate that the Akt pathway strongly responds to Alzheimer's disease in hippocampus, in an age-dependent manner. We observed a strong increase of phosphorylated Akt, S6 and ERK in the early phase of the pathology, while they were less activated during the late stages. Differences may be ascribed to the exacerbation of the amyloid pathology and/or to a differential contribution of hippocampal cell types to signalling with increasing age. Interestingly, functional *ex vivo* studies reported that activation of the PI3K-Akt pathway is reduced, due to serine inhibition of IRS-1 in the brains of Alzheimer's disease patients and of Alzheimer's disease mouse models (Bomfim *et al.*, 2012; Talbot *et al.*, 2012), which may reflect a disease stage where protective mechanisms failed and neurons are overwhelmed by amyloid-β pathology. Therefore, brain IGF1 resistance observed post-mortem in Alzheimer's disease is possibly not the primary cause but rather represents a residual defence mechanism for surviving neurons to limit damage due to amyloid-β proteotoxicity (Bomfim *et al.*, 2012; Talbot *et al.*, 2012). This hypothesis is in agreement with our microarray data showing that several genes reported to

be neuroprotective in Alzheimer's disease were upregulated in early stage AD mice neurons, namely *Ttr*, *Grk5* and *Dhcr24*. Interestingly, the expression of these genes were normalized to wild-type levels in ADINKO neurons, indicating that neuroprotective responses were not activated at this stage, possibly because restored neuronal homeostasis staved off Alzheimer's disease. Indeed, hemizygous deletion of *Ttr* gene exacerbated amyloidosis, whereas overexpression of TTR reduced amyloid-β load and improved cognition in Alzheimer's disease mice (Choi *et al.*, 2007; Buxbaum *et al.*, 2008; Li *et al.*, 2011). Protective activity of TTR stems from its capacity to bind amyloid-β aggregates in both the intracellular and extracellular environment in a chaperone-like manner. Recently, Li *et al.* (2016) reported that TTR's interaction with amyloid-β involve the C99 fragment of APP, and a positive link between TTR abundance in the brain and local IGF1R gene expression was discovered by Vieira *et al.* (2015). This is compatible with our findings, yet reciprocal regulation has not been demonstrated so far. Similarly, membrane G protein-coupled receptor kinase 5 deficiency in Alzheimer's disease mice exaggerated neuroinflammation and amyloid burden (Li *et al.*, 2008; Cheng *et al.*, 2010). Finally, the cholesterol synthesizing enzyme DHCR24 has been shown to be neuroprotective by modulating cholesterol concentration in lipid raft membranes, which could directly influence amyloid-β synthesis by altering interactions between the APP precursor and its cleaving enzymes (Peri and Serio, 2008; Hernández-Jiménez *et al.*, 2016).

Inactivating neuronal IGF1R enhances neuronal resistance to proteotoxicity through coordinated changes in selected cell functions

Ablation of IGF1R from differentiated neurons regulated mainly genes involved in cell growth, cytoskeleton organization, neurotransmission and proteostasis. Changes in gene pathways related to cell growth and proteostasis are in agreement with reduction in soma size, specifically of apical cytoplasm and primary dendrite in response to IGF1R deletion (Gontier *et al.*, 2015), or after interfering with downstream PI3k-Akt-mTOR signalling in mice (Tavazoie *et al.*, 2005; Cloetta *et al.*, 2013; Thomanetz *et al.*, 2013; Goebbels *et al.*, 2017). In humans, activating mutations in mTOR have also been reported in developmental disorders including megalencephaly and focal cortical dysplasia, and have been associated with increased neuronal soma size (Mirzaa *et al.*, 2016). Regarding cytoskeleton organization, *Nefm* is particularly interesting because it is one of the three genes consistently affected when comparing the transcriptomes of neurons altered by IGF1R deletion, Alzheimer's disease and the interaction between the disease and IGF1R deletion. Indeed, we showed that suppression of neuronal IGF1R led to significant reduction in hippocampal NEFM protein. Together with the neurofilament heavy (NEFH) and light (NEFL) polypeptides, they form the 10-nm intermediate filaments of mature neurons, and play pivotal roles in axonal and dendritic branching and growth. NEFM is especially critical for determining calibre of myelinated axons (Garcia *et al.*, 2003). Notably, NEFL abundance in blood and CSF has recently been identified as a biomarker of disease development and response to treatment in Alzheimer's disease since NEFL concentration concurred with progression of proteopathy-induced neurodegeneration (Bacioglu *et al.*, 2016). We found increased amounts of NEFM in hippocampus of AD mice, in agreement with previous results showing accumulation of neurofilaments in Alzheimer's disease brain (Deng *et al.*, 2008). Abnormal accumulation of neurofilaments and destabilization of associated microtubules are often connected in neurodegenerative disorders (Yadav *et al.*, 2016). Depletion of axonal neurofilaments or removal of the hyperphosphorylated tail domain of NEFM and NEFH have been shown to retard onset and slow down progression of amyotrophic lateral sclerosis, and ameliorate motor neuron survival. Alleviation of motor neuron toxicity has been ascribed to improvement in microtubule dynamics leading to enhanced axonal transport of mitochondria and lysosomes (Perrot and Julien, 2009; Yadav *et al.*, 2016). Therefore, we postulate that reduction in NEFM expression in ADINKO and inIGF1RKO mice contributes to the improvement in neuronal function, probably through facilitated axonal transport. Soma being the primary site of degradation of autophagic cargo (Maday and Holzbaur, 2016), this could explain the improved autophagic compartment, namely reduced accumulation of amyloid-β containing autophagic vacuoles around the peri-nuclear regions that we observed in ADINKO hippocampus compared to AD mice (Gontier *et al.*, 2015). Moreover, NEFM has been shown to anchor dopamine receptor 1-containing endosomes within synapses, which could facilitate rapid receptor recycling to the synaptic membrane following stimulation by dopamine agonists (Yuan *et al.*, 2015). Yuan and coworkers showed *in vivo* that in the absence of NEFM, there was increased recycling back to the membrane, leading to dopamine receptor hypersensitivity. Thus, changes in cytoskeleton organization in our mutants could also contribute to enhanced postsynaptic neurotransmission. This is in agreement with increased AMPAR and NMDAR-dependent excitability of hippocampal neurons that we previously demonstrated in a related model of conditional neuronal inactivation of IGF1R (De Magalhaes Filho *et al.*, 2017). Indeed, neurotransmission appeared as a major pathway affected by IGF1R deletion and by Alzheimer's disease in our transcriptome analysis. Accordingly, we found that phospho-activation of CREB, which is required for long-term plasticity and memory formation (Benito and Barco, 2010; Alberini and Kandel, 2014), increased in hippocampus in the absence of IGF1R. Gazit and colleagues (2016) recently demonstrated that basal IGF1R activity enhances evoked synaptic transmission while inhibiting spontaneous

transmission. In agreement with our *in vivo* data, these authors also showed that IGF1R blockade rescued Alzheimer's disease-associated hippocampal hyperactivity to wild-type levels (Gazit *et al.*, 2016).

Altogether, we demonstrated that resistance of the brain to proteotoxicity can be achieved lifelong by inhibiting neuronal IGF1R. We also identified a convergent transcriptomic signature of early-stage Alzheimer's disease neurons and adult-onset IGF1R-deficient neurons that are resistant to amyloid-β proteotoxicity, highlighting similar genetically regulated defence mechanisms of the neuron. Our data further indicate that suppression of IGF signals in mature neurons triggers cytoskeleton and soma size remodelling, which improves synaptic transmission and optimizes protein recycling in proteinopathies. This enhanced homeostasis confers extended intrinsic neuroprotective capacities against proteotoxic lesions during ageing, suggesting that suppression of IGF signals in adult neurons represents a relevant prevention strategy in people at risk for Alzheimer's disease.

Acknowledgements

The authors thank Camille Legout, Tatiana Ledent and coworkers of the mouse facility PHEA, and Franck Letourneur, Sebastien Jacques and coworkers of the GENOM'IC platform at Institut Cochin, Paris.

Funding

This work was funded by INSERM cross-cutting program on ageing, UPMC, France Alzheimer, and *Ligue Européenne Contre la Maladie d'Alzheimer* (LECMA - Vaincre Alzheimer). Fellowships to C.G., G.G. and S.A. were provided by *Ministère de l'Enseignement Supérieur et de la Recherche* (MESR), *Fondation pour la Recherche Médicale* (FRM) and *Fondation Plan Alzheimer*. The authors declare no competing financial interests and no other conflict of interest.

Supplementary material

Supplementary material is available at *Brain* online.

References

Aid S, Langenbach R, Bosetti F. Neuroinflammatory response to lipopolysaccharide is exacerbated in mice genetically deficient in cyclooxygenase-2. J Neuroinflammation 2008; 5: 17.

Alberini CM, Kandel ER. The regulation of transcription in memory consolidation. Cold Spring Harb Perspect Biol 2014; 7: a021741.

Andreasson KI, Bachstetter AD, Colonna M, Ginhoux F, Holmes C, Lamb B, et al. Targeting innate immunity for neurodegenerative disorders of the central nervous system. J Neurochem 2016; 138: 653–93.

Bacioglu M, Maia LF, Preische O, Schelle J, Apel A, Kaeser SA, et al. Neurofilament light chain in blood and CSF as marker of disease progression in mouse models and in neurodegenerative diseases. Neuron 2016; 91: 56–66.

Benito E, Barco A. CREB's control of intrinsic and synaptic plasticity: implications for CREB-dependent memory models. Trends Neurosci 2010; 33: 230–40.

Biondi O, Branchu J, Ben Salah A, Houdebine L, Bertin L, Chali F, et al. IGF-1R reduction triggers neuroprotective signaling pathways in spinal muscular atrophy mice. J Neurosci 2015; 35: 12063–79.

Bomfim TR, Forny-Germano L, Sathler LB, Brito-Moreira J, Houzel JC, Decker H, et al. An anti-diabetes agent protects the mouse brain from defective insulin signaling caused by Alzheimer's disease- associated Abeta oligomers. J Clin Invest 2012; 122: 1339–53.

Buxbaum JN, Ye Z, Reixach N, Friske L, Levy C, Das P, et al. Transthyretin protects Alzheimer's mice from the behavioral and biochemical effects of Abeta toxicity. Proc Natl Acad Sci USA 2008; 105: 2681–86.

Byrne AB, Walradt T, Gardner KE, Hubbert A, Reinke V, Hammarlund M. Insulin/IGF1 signaling inhibits age-dependent axon regeneration. Neuron 2014; 81: 561–73.

Cheng S, Li L, He S, Liu J, Sun Y, He M, et al. GRK5 deficiency accelerates {beta}-amyloid accumulation in Tg2576 mice via impaired cholinergic activity. J Biol Chem 2010; 285: 41541–8.

Choi SH, Bosetti F. Cyclooxygenase-1 null mice show reduced neuroinflammation in response to beta-amyloid. Aging 2009; 1: 234–44.

Choi SH, Leight SN, Lee VM-Y, Li T, Wong PC, Johnson JA, et al. Accelerated Abeta deposition in APPswe/PS1deltaE9 mice with hemizygous deletions of TTR (transthyretin). J Neurosci 2007; 27: 7006–10.

Clarke JR, Lyra e Silva NM, Figueiredo CP, Frozza RL, Ledo JH, Beckman D, et al. Alzheimer-associated Aβ oligomers impact the central nervous system to induce peripheral metabolic deregulation. EMBO Mol Med 2015; 7: 190–210.

Cloetta D, Thomanetz V, Baranek C, Lustenberger RM, Lin S, Oliveri F, et al. Inactivation of mTORC1 in the developing brain causes microcephaly and affects gliogenesis. J Neurosci 2013; 33: 7799–810.

Cohen E, Bieschke J, Perciavalle RM, Kelly JW, Dillin A. Opposing activities protect against age-onset proteotoxicity. Science 2006; 313: 1604–10.

Cohen E, Paulsson JF, Blinder P, Burstyn-Cohen T, Du D, Estepa G, et al. Reduced IGF-1 signaling delays age-associated proteotoxicity in mice. Cell 2009; 139: 1157–69.

Dansokho C, Ait Ahmed D, Aid S, Toly-Ndour C, Chaigneau T, Calle V, et al. Regulatory T cells delay disease progression in Alzheimer-like pathology. Brain 2016; 139: 1237–51.

De Magalhaes Filho CD, Kappeler L, Dupont J, Solinc J, Villapol S, Denis C, et al. Deleting IGF-1 receptor from forebrain neurons confers neuroprotection during stroke and upregulates endocrine somatotropin. J Cereb Blood Flow Metab 2017; 37: 396–412.

Deng Y, Li B, Liu F, Iqbal K, Grundke-Iqbal I, Brandt R, et al. Regulation between O-GlcNAcylation and phosphorylation of neurofilament-M and their dysregulation in Alzheimer disease. FASEB J 2008; 22: 138–45.

Ferreira ST, Lourenco MV, Oliveira MM, De Felice FG. Soluble amyloid-β oligomers as synaptotoxins leading to cognitive impairment in Alzheimer's disease. Front Cell Neurosci 2015; 9: 191.

Florez-McClure ML, Hohsfield LA, Fonte G, Bealor MT, Link CD. Decreased insulin-receptor signaling promotes the autophagic degradation of beta-amyloid peptide in C. elegans. Autophagy 2007; 3: 569–80.

Freude S, Hettich MM, Schumann C, Stohr O, Koch L, Kohler C, et al. Neuronal IGF-1 resistance reduces Abeta accumulation and protects against premature death in a model of Alzheimer's disease. FASEB J 2009; 23: 3315–24.

Garcia ML, Lobsiger CS, Shah SB, Deerinck TJ, Crum J, Young D, et al. NF-M is an essential target for the myelin-directed 'outside-in' signaling cascade that mediates radial axonal growth. J Cell Biol 2003; 163: 1011–20.

Gazit N, Vertkin I, Shapira I, Helm M, Slomowitz E, Sheiba M, et al. IGF-1 receptor differentially regulates spontaneous and evoked transmission via mitochondria at hippocampal synapses. Neuron 2016; 89: 583–97.

Ginsberg SD, Alldred MJ, Che S. Gene expression levels assessed by CA1 pyramidal neuron and regional hippocampal dissections in Alzheimer's disease. Neurobiol Dis 2012; 45: 99–107.

Goebbels S, Wieser GL, Pieper A, Spitzer S, Weege B, Yan K, et al. A neuronal PI(3,4,5)P3-dependent program of oligodendrocyte precursor recruitment and myelination. Nat Neurosci 2017; 20: 10–15.

Gontier G, George C, Chaker Z, Holzenberger M, Aïd S. Blocking IGF signaling in adult neurons alleviates Alzheimer's disease pathology through amyloid-β clearance. J Neurosci 2015; 35: 11500–13.

Herculano-Houzel S, Mota B, Lent R. Cellular scaling rules for rodent brains. Proc Natl Acad Sci USA 2006; 103: 12138–43.

Hernández-Jiménez M, Martínez-López D, Gabandé-Rodríguez E, Martín-Segura A, Lizasoain I, Ledesma MD, et al. Seladin-1/DHCR24 is neuroprotective by associating EAAT2 glutamate transporter to lipid rafts in experimental stroke. Stroke 2016; 47: 206–13.

Holzenberger M, Dupont J, Ducos B, Leneuve P, Geloen A, Even PC, et al. IGF-1 receptor regulates lifespan and resistance to oxidative stress in mice. Nature 2003; 421: 182–7.

Jankowsky JL, Fadale DJ, Anderson J, Xu GM, Gonzales V, Jenkins NA, et al. Mutant presenilins specifically elevate the levels of the 42 residue beta-amyloid peptide *in vivo*: evidence for augmentation of a 42-specific gamma secretase. Hum Mol Genet 2004; 13: 159–70.

Kappeler L, De Magalhaes Filho C, Dupont J, Leneuve P, Cervera P, Périn L, et al. Brain IGF-1 receptors control mammalian growth and lifespan through a neuroendocrine mechanism. PLoS Biol 2008; 6: e254.

Kenyon CJ. The genetics of ageing. Nature 2010; 464: 504–12.

Landel V, Baranger K, Virard I, Loriod B, Khrestchatisky M, Rivera S, et al. Temporal gene profiling of the 5XFAD transgenic mouse model highlights the importance of microglial activation in Alzheimer's disease. Mol Neurodegener 2014; 9: 33.

Leinenga G, Götz J. Scanning ultrasound removes amyloid-β and restores memory in an Alzheimer's disease mouse model. Sci Transl Med 2015; 7: 278ra33.

Lesné SE, Sherman MA, Grant M, Kuskowski M, Schneider JA, Bennett DA, et al. Brain amyloid-β oligomers in ageing and Alzheimer's disease. Brain 2013; 136: 1383–98.

Li L, Liu J, Suo WZ. GRK5 deficiency exaggerates inflammatory changes in TgAPPsw mice. J Neuroinflammation 2008; 5: 24.

Li X, Masliah E, Reixach N, Buxbaum JN. Neuronal production of transthyretin in human and murine Alzheimer's disease: is it protective? J Neurosci 2011; 31: 12483–90.

Li X, Song Y, Sanders CR, Buxbaum JN. Transthyretin suppresses amyloid-β secretion by interfering with processing of the amyloid-β protein precursor. J Alzheimers Dis 2016; 52: 1263–75.

Liaury K, Miyaoka T, Tsumori T, Furuya M, Wake R, Ieda M, et al. Morphological features of microglial cells in the hippocampal dentate gyrus of Gunn rat: a possible schizophrenia animal model. J Neuroinflammation 2012; 9: 56.

Longo VD, Antebi A, Bartke A, Barzilai N, Brown-Borg HM, Caruso C, et al. Interventions to slow aging in humans: are we ready? Aging Cell 2015; 14: 497–510.

Maday S, Holzbaur ELF. Compartment-specific regulation of autophagy in primary neurons. J Neurosci 2016; 36: 5933–45.

Milman S, Huffman DM, Barzilai N. The somatotropic axis in human aging:framework for the current state of knowledge and future research. Cell Metab 2016; 23: 980–9.

Mirzaa GM, Campbell CD, Solovieff N, Goold CP, Jansen LA, Menon S, et al. Association of MTOR mutations with developmental brain disorders, including megalencephaly, focal cortical dysplasia, and pigmentary mosaicism. JAMA Neurol 2016; 73: 836–45.

Moloney AM, Griffin RJ, Timmons S, O'Connor R, Ravid R, O'Neill C. Defects in IGF-1 receptor, insulin receptor and IRS-1/2 in Alzheimer's disease indicate possible resistance to IGF-1 and insulin signalling. Neurobiol Aging 2010; 31: 224–43.

Paxinos G, Franklin K. The mouse brain in stereotaxic coordinates, . San Diego, CA: Elsevier; 2013.

Peri A, Serio M. Neuroprotective effects of the Alzheimer's disease-related gene seladin-1. J Mol Endocrinol 2008; 41: 251–61.

Perrot R, Julien JP. Real-time imaging reveals defects of fast axonal transport induced by disorganization of intermediate filaments. FASEB J 2009; 23: 3213–25.

Santos DB, Peres KC, Ribeiro RP, Colle D, dos Santos AA, Moreira ELG, et al. Probucol, a lipid-lowering drug, prevents cognitive and hippocampal synaptic impairments induced by amyloid β peptide in mice. Exp Neurol 2012; 233: 767–75.

Steen E, Terry BM, Rivera EJ, Cannon JL, Neely TR, Tavares R, et al. Impaired insulin and insulin-like growth factor expression and signaling mechanisms in Alzheimer's disease–is this type 3 diabetes? J Alzheimers Dis 2005; 7: 63–80.

Talbot K, Wang HY, Kazi H, Han LY, Bakshi KP, Stucky A, et al. Demonstrated brain insulin resistance in Alzheimer's disease patients is associated with IGF-1 resistance, IRS-1 dysregulation, and cognitive decline. J Clin Invest 2012; 122: 1316–38.

Tavazoie SF, Alvarez VA, Ridenour DA, Kwiatkowski DJ, Sabatini BL. Regulation of neuronal morphology and function by the tumor suppressors Tsc1 and Tsc2. Nat Neurosci 2005; 8: 1727–34.

Thomanetz V, Angliker N, Cloetta D, Lustenberger RM, Schweighauser M, Oliveri F, et al. Ablation of the mTORC2 component rictor in brain or Purkinje cells affects size and neuron morphology. J Cell Biol 2013; 201: 293–308.

Tramutola A, Triplett JC, Di Domenico F, Niedowicz DM, Murphy MP, Coccia R, et al. Alteration of mTOR signaling occurs early in the progression of Alzheimer disease (AD): analysis of brain from subjects with pre-clinical AD, amnestic mild cognitive impairment and late-stage AD. J Neurochem 2015; 133: 739–49.

Vieira M, Gomes JR, Saraiva MJ. Transthyretin induces insulin-like growth factor I nuclear translocation regulating its levels in the hippocampus. Mol Neurobiol 2015; 51: 1468–79.

Xu J, Gontier G, Chaker Z, Lacube P, Dupont J, Holzenberger M. Longevity effect of IGF-1R(+/-) mutation depends on genetic background-specific receptor activation. Aging Cell 2014; 13: 19–28.

Yadav P, Selvaraj BT, Bender FLP, Behringer M, Moradi M, Sivadasan R, et al. Neurofilament depletion improves microtubule dynamics via modulation of Stat3/stathmin signaling. Acta Neuropathol 2016; 132: 93–110.

Yuan A, Sershen H, Veeranna, Basavarajappa BS, Kumar A, Hashim A, et al. Neurofilament subunits are integral components of synapses and modulate neurotransmission and behavior *in vivo*. Mol Psychiatry 2015; 20: 986–94.